ORIGINAL ARTICLE

Response to radiotherapy in pancreatic ductal adenocarcinoma is enhanced by inhibition of myeloid-derived suppressor cells using STAT3 anti-sense oligonucleotide

Ayman J. Oweida[1] · Adam C. Mueller[11] · Miles Piper[10] · Dallin Milner[10] · Benjamin Van Court[10] · Shilpa Bhatia[10] · Andy Phan[10] · Thomas Bickett[10] · Kimberly Jordan[9] · Theresa Proia[2] · Richard Schulick[3] · Wells A. Messersmith[4] · Marco Del Chiaro[3] · Eric Clambey[5] · Michael J. Gough[6] · Jason Williams[7] · Kirk Hansen[7] · Karyn Goodman[8] · Sana D. Karam[1,10]

Abstract

Pancreatic ductal adenocarcinoma (PDAC) has a heterogeneous tumor microenvironment (TME) comprised of myeloid-derived suppressor cells (MDSCs), tumor-associated macrophages, neutrophils, regulatory T cells, and myofibroblasts. The precise mechanisms that regulate the composition of the TME and how they contribute to radiotherapy (RT) response remain poorly understood. In this study, we analyze changes in immune cell populations and circulating chemokines in patient samples and animal models of pancreatic cancer to characterize the immune response to radiotherapy. Further, we identify STAT3 as a key mediator of immunosuppression post-RT. We found granulocytic MDSCs (G-MDSCs) and neutrophils to be increased in response to RT in murine and human PDAC samples. We also found that RT-induced STAT3 phosphorylation correlated with increased MDSC infiltration and proliferation. Targeting STAT3 using an anti-sense oligonucleotide in combination with RT circumvented RT-induced MDSC infiltration, enhanced the proportion of effector T cells, and improved response to RT. In addition, STAT3 inhibition contributed to the remodeling of the PDAC extracellular matrix when combined with RT, resulting in decreased collagen deposition and fibrotic tissue formation. Collectively, our data provide evidence that targeting STAT3 in combination with RT can mitigate the pro-tumorigenic effects of RT and improve tumor response.

Introduction

Pancreatic ductal adenocarcinoma (PDAC) is the fourth leading cause of cancer-related deaths in the world [1] with a dismal 5-year overall survival (OS) rate of 8% [2]. Approximately 30% of PDAC patients present with locally advanced (LA) disease and are deemed inoperable. Limited targeted therapies are available for LA-PDAC patients [3] and response to single-agent immunotherapy has been

disappointing with new combinatorial approaches yet to show benefit [4]. Therefore, non-surgical approaches are limited to chemotherapy and radiotherapy (RT). Although some retrospective analyses and national registry studies have shown a survival benefit with the addition of RT preoperatively in locally advanced pancreatic cancer (LAPC) [5], the LAP07 international phase three trial demonstrated no significant benefit in OS in patients with LAPC following long-course chemoradiotherapy compared to chemotherapy alone (median OS 15.2 vs 16.5 months, respectively; $p = 0.83$).

Recent advances in the effort to enhance the efficacy of radiotherapy have recognized the importance of the immune system in mediating the response. In addition to promoting T cell priming, radiation recruits suppressive immune populations such as myeloid-derived suppressor cells (MDSCs) and regulatory T cells (Tregs) to the tumor microenvironment

✉ Sana D. Karam
sana.karam@cuanschutz.edu

Extended author information available on the last page of the article

(TME) in a variable and spatiotemporal manner [6, 7]. This is highly relevant to PDAC where the TME is, at baseline, primarily comprised of MDSCs, tumor-associated macrophages (TAMs), neutrophils, Tregs, and myofibroblasts. These populations have the capacity to blunt RT-induced anti-tumor immune responses by blocking the activity of effector CD4^{+} and CD8^{+} T cells [8, 9]. RT can also contribute to the formation of fibrotic stroma by stimulating the recruitment of stromal fibroblasts and their transdifferentiation into cancer associated fibroblasts (CAFs), resulting in increased collagen deposition and the induction of a reactive stroma that both promotes tumor growth [10–12] and acts as a barrier to intratumoral effector T cell infiltration [13, 14]. Therefore, identifying targets that can limit RT-induced immunosuppression and fibrosis have significant therapeutic implications in enhancing response to RT. In this study, we identify STAT3 as an important mediator of immunosuppression in PDAC. We show STAT3 blockade significantly reduces RT-induced fibrosis and enhances anti-tumor immunity. Our data provide new insight into mechanisms of radioresistance and should guide the design of clinical trials aimed at improving response to RT in LAPC patients.

Materials and methods

Cell lines and cell culture

Mouse KPC pancreatic cancer cell lines FC1242 and PK5L1940 cells were cultured in DMEM-F12 media supplemented with 10% FBS and 1% primocin.

Animal tumor model

Female C57BL/6 and nude mice age 5–8 weeks were purchased from Jackson Labs (ME). Cell suspensions of equal parts media and Matrigel (10 mg/mL, BD Biosciences, San Jose, CA) were injected at a final concentration of $1\times10^6/0.1$ mL at a single site in the right flank of each animal. Treatment was started when average tumor size reached 100mm^3. Mice exhibiting signs of morbidity were sacrificed according to the guidelines set by the Institutional Animal Care and Use Committee (IACUC). All protocols for animal tumor models were approved by the IACUC of the University of Colorado Denver.

Antibodies and drugs

For STAT3 inhibition, the synthetic anti-sense oligonucleotide (ASO) targeting murine STAT3 was used (481,549, Ionis Pharmaceuticals). Mice were dosed with mouse STAT3 ASO or control ASO at 50 mg/kg diluted in sterile saline 5 times per week, subcutaneously, starting at 3 days prior to RT and maintained for 2 weeks.

Irradiation

Irradiation was performed using the X-RAD SmART image-guided irradiator (Precision X-Ray Inc., Bradford CT) at 225kVp, 20 mA with 0.3 mm Cu filter. CBCT scans of representative mice were acquired and Monte-Carlo simulations performed using SmART-ATP software to determine the appropriate beam-on time. Mice were positioned using fluoroscopy to ensure accurate targeting prior to radiation delivery at a dose rate of 5.6 Gy/min. Monthly QA testing was performed using an ionization chamber to ensure a consistent dose rate from the irradiator.

Flow cytometry

For flow cytometric analysis of tumor tissue, tumors were digested into single-cell suspension as previously reported [15]. Briefly, tumors, were finely cut and incubated in Collagenase III solution (Worthington). After incubation, tumors were passed through a 70 µm nylon mesh. The resulting cell suspension was centrifuged and re-suspended in red blood cell lysis buffer for 2 min. RBC lysis buffer was deactivated, cell suspensions were centrifuged, re-suspended, and counted using an automated cell counter. Trypan blue was used to determine cell viability. Draining lymph nodes and spleens were processed in a similar manner. For flow cytometric analysis, 1×10^6 live cells were plated in 24-well plates and cultured for 5 h in the presence of monensin, PMA, and ionomycin to stimulate cytokine production and block their release. Cells were then blocked with anti-CD16/32 antibody. For analysis of immune cells, the following conjugated antibodies were used: APC-eFluor780-CD8 (Clone 53-6.7, eBioscience), eFluor450-CD4 (Clone RM4-5, eBioscience) AlexaFluor700-CD45 (Clone 30-F11, eBioscience), DyLight350-CD3 (Clone 145-2C11, Novus), FITC-CD44 (Clone IM7, eBioscience), PECyanine7-IFNγ (Clone XMG1.2, eBioscience), APC or APC-eFluor780—Ki67 (Clone 16A8 eBioscience), PE-CD25 (Clone 3C7, BioLegend), PerCP-Cy5.5-F4/80 (Clone BM8, eBioscience), PE-Cyanin7-CD11b (Clone M1/70, eBioscience), BV421-Gr1 (Clone RB6-8C5, BioLegend), FITC-CD163 (6E10.1G6, Bioss Antibodies), APC-iNOS (Clone CXNFT, eBioscience), and PE-pSTAT3 (pS727) (Clone 49, BD Biosciences). Where necessary, cells were fixed and permeabilized prior to staining using the Lyse/Fix 5X and BD Phosflow Perm Buffer III (BD Biosciences). Gating strategies provided in Supplementary Fig. 1a. Samples were run on the Yeti Cell Analyzer at the University of Colorado Denver Cancer Flow Cytometry Core. Data were analyzed using FlowJo Analysis software.

Mass cytometry (CyTOF)

Mass cytometry by time-of-flight (CyTOF) analysis was performed on human peripheral blood mononuclear cells (PBMCs). Cells were stained with the following heavy-metal tagged antibodies: CD19-142Nd, CD11c-162Dy, CD127-149Sm, CD16-209Bi, CD25-169Tm, CD27-155Gd, CD45-89Y, CD3e-154Sm, CD4-174Yb, CD8a-168Er, CD11b-153Eu, FoxP3-165Ho, CD15-164Dy, Intercalator Ir-191/Ir-193, and Cisplatin-Pt-195. Samples were run on the Helios Mass Cytometer at the University of Colorado Denver Cancer Center Flow Cytometry Core. Gating was performed on nucleated live cells. Data was analyzed using FlowJo Analysis software.

ELISA and multiplex secretome assays

Mouse plasma was subjected to R&D Systems (MN) Mouse/Rat/Porcine/Canine TGF-β1 Quantikine ELISA Kit as per manufacturer's instructions. Patient blood samples were collected as part of a Phase I radiation dose-escalation clinical trial (NCT02873598). Blood samples were obtained at 3 timepoints: Baseline (within 14 days of SBRT), during (the week the three fractions of SBRT were delivered) and post (6 weeks ± 1 week after SBRT). Human plasma samples were analyzed on the V-PLEX Human Cytokine 30-plex kit [MesoScale Diagnostics (MD)] by the University of Colorado Human Immune Monitoring Shared Resource. All human studies were performed after approval by the University of Colorado institutional review board (COMIRB16-1139) and written informed consent was obtained from all patients as dictated by the study protocol.

Immunohistochemistry

Harvested tumor tissue was formalin-fixed and paraffin embedded. 4–6 μm thick sections were deparaffinized with xylene and rehydrated with decreasing concentrations of ethanol. For IHC, heat-mediated antigen retrieval was performed using citrate buffer. Tissues were blocked with 2% milk in TBS-Triton-X for 30 min at room temperature and stained with primary antibodies at room temperature overnight. PicroSirius Red staining was performed as described previously and counterstained with Weigert's hematoxylin. Processing of tissues for PicroSirius Red staining was completed by the University of Colorado Denver Research Histology Shared Resource. Images were captured using a Nikon microscope. PicroSirius images were captured with Nikon Eclipse Ni Microscope and DS-Ri2 Camera with Nikon Elements D software through a Nikon Plan Fluor 10X/0.30 objective. Quantification of scanned images was performed using NIH ImageJ software on 3–5 tumors per treatment group per tumor model. 5–8 fields per slide were chosen and analyzed by quantifying the percentage of fibrosis compared to the total amount of tissue within the image as previously described [16].

Mass spectrometry

Briefly, snap frozen tumor samples of approximately 5 mg were powderized in liquid nitrogen. High salt extraction was used to make the cell fraction. Guanidine extraction was used to make the sECM fraction. Hydroxylamine extraction was used to make the iECM fraction. Fractions were digested with trypsin. 600 ng of protein was analyzed nano-UHPLC-MS/MS (Easy-nLC1200, Orbitrap Fusion™ Lumos™ Tribrid™, Thermo Fisher Scientific). Files were loaded into Proteome Discoverer 2.2 and were searched against the Swissprot mouse and human database. In Excel, protein abundances from the three fractions were summed together for each protein. Data was visualized in excel and MetaboAnalyst 4.0 [17].

Statistical analysis

Two-way analysis of variance (ANOVA) was performed to assess differences in the expression of markers across treatment groups. Unpaired two-tailed Student's t test was used for analysis of flow cytometry data. For survival analysis, Kaplan–Meier curves were analyzed with Log-rank (Mantel-Cox) test for comparison of groups. For assessment of tumor growth differences, 2-way ANOVA was performed. All statistical analyses were performed in Prism software (GraphPad, v6.00).

Results

Immunosuppressive myeloid cells and chemokines are increased in PDAC patients after RT

In order to characterize the suppressive immune response following RT, we analyzed blood samples from seven PDAC patients at baseline, during, and after RT and assessed changes in plasma chemokines and immune cell populations. Analysis of myeloid cells (CD45$^+$CD11b$^+$) showed significant increases in MSDCs (CD11b$^+$CD33$^+$) during and after RT relative to baseline (Fig. 1a). No significant differences were observed in macrophage (CD11b$^+$CD16$^+$), CD8 T cell, CD4 T cell, or regulatory T cell populations throughout treatment (Fig. 1a). We further assessed levels of phosphorylated STAT3, which is involved in promoting secretion of immunosuppressive chemokines [18]. MDSCs and monocytes showed the highest proportion of phosphorylated STAT3 (mean ± SEM: 51.73 ± 6.51% and 31.80 ± 5.26% respectively). Within
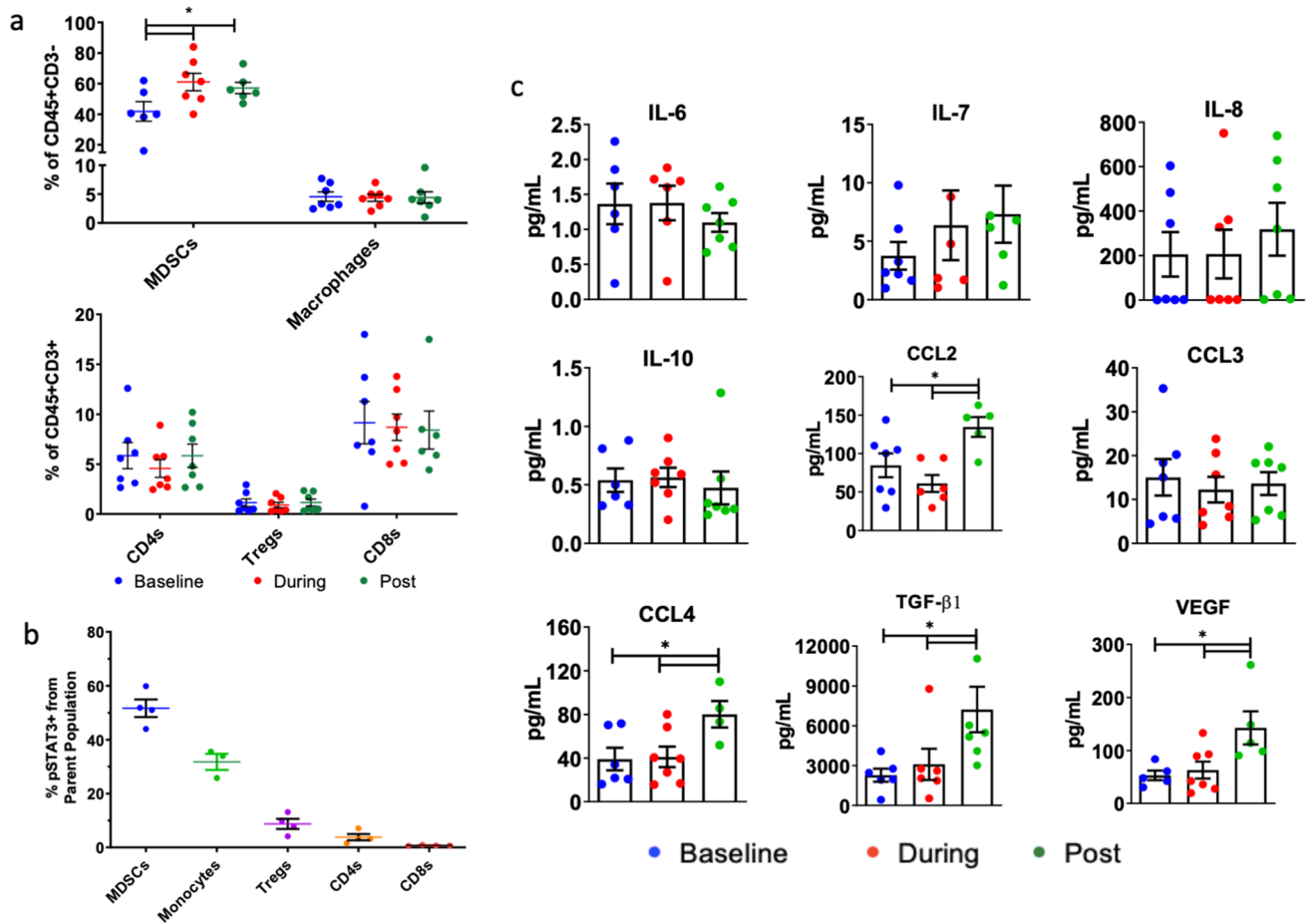
Fig. 1 Analysis of PBMCs from PDAC patients shows significant upregulation of immune chemokines and changes in immune populations. **a** CyTOF analysis shows elevated levels of circulating MDSCs during and post-RT. **b** CyTOF analysis shows the highest expression of pSTAT3 to be on MDSCs and monocytes. **c** Multiplex chemokine analysis using the Mesoscale platform shows significant induction of CCL2, CCL4, VEGF and TGF-β1 post-RT. Asterisks denote significance ($p < 0.05$) in comparison to all groups (two-way ANOVA). Bars represent standard error of the mean

the T cell population, $8.73 \pm 3.4\%$ of Tregs expressed pSTAT3 while $3.83 \pm 2.3\%$ and $0.74 \pm 0.15\%$ of CD4 and CD8 T cells expressed pSTAT3, respectively (Fig. 1b). Analysis of patient plasma samples revealed significant changes in immune-related chemokines during the course of therapy. CCL2 (MCP-1) and CCL4 (MIP-1β) were significantly increased after RT compared to baseline and during RT (Fig. 1c). Levels of vascular endothelial growth factor (VEGF), which is involved in angiogenesis and monocyte recruitment [19], were significantly increased after RT compared to baseline and during RT (Fig. 1c). In addition, TGF-β1 was significantly increased after RT compared to baseline and during RT. No changes were observed in IL-6 or IL-10 levels during any stage of treatment (Fig. 1c).

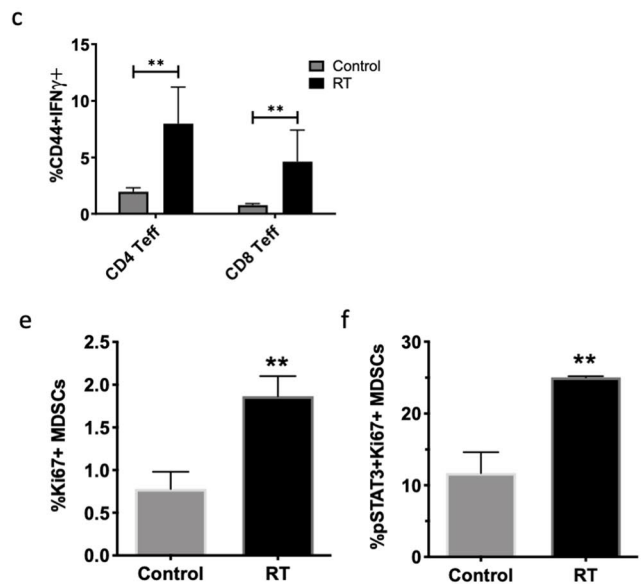## RT creates an immunosuppressive myeloid cell-rich microenvironment in murine PDAC

To identify changes in the tumor microenvironment in response to RT, we inoculated mice with FC1242 Kras-driven PDAC and allowed tumors to reach 400 mm³ before irradiating with a dose of 8 Gy. Tumors were harvested 96 h later (Fig. 2a). Analysis of intratumoral immune populations in murine FC1242 tumors showed significant changes in immunosuppressive myeloid populations. The total MDSC ($CD11b^+Gr1^+$) population increased by 3.15-fold following radiation, with G-MDSCs ($CD11b^+Ly6C^{low}Ly6G^+$) increasing by 4.5-fold and M-MDSCs ($CD11b^+Ly6C^{high}Ly6G^-$) increasing by 3.0-fold (Fig. 2a). In addition, neutrophils ($CD11b^+Ly6C^-Ly6G^+$) increased by 2.59-fold and myeloid
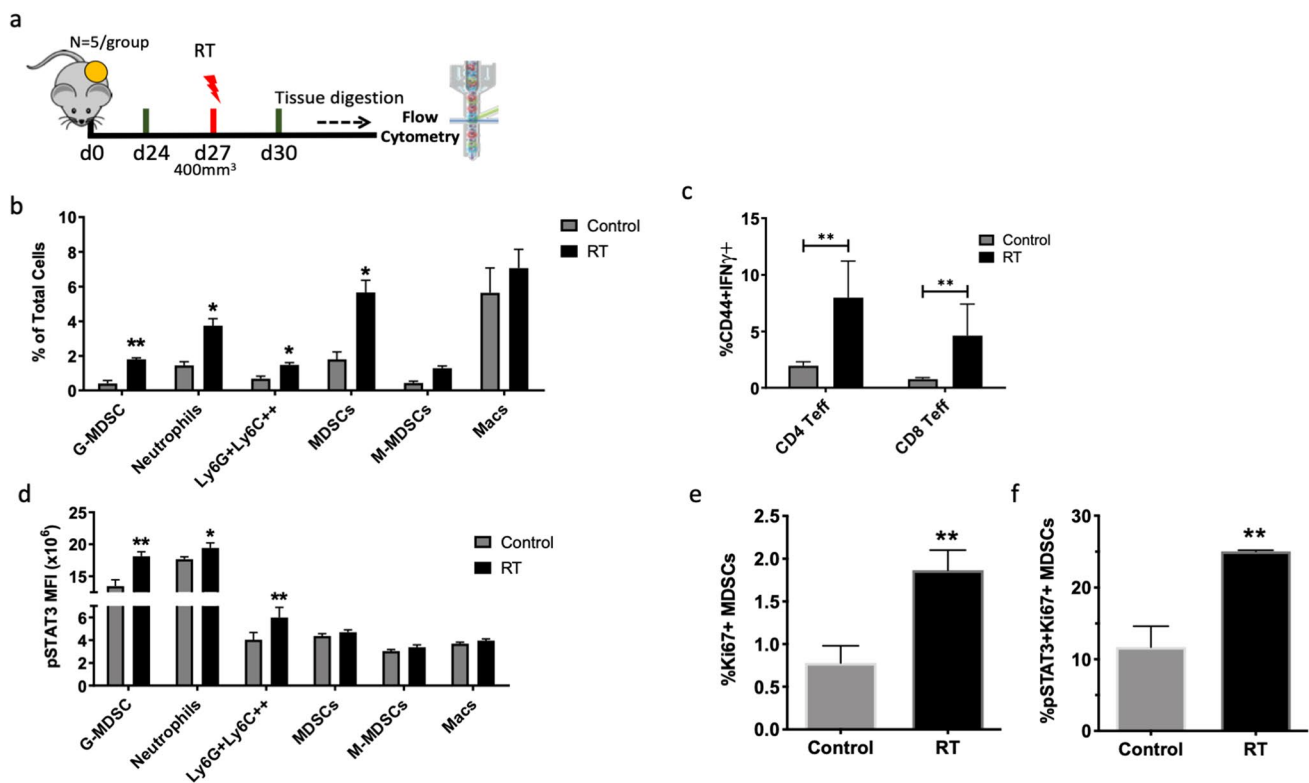
Fig. 2 Radiotherapy enhances myeloid-derived suppressor cell populations intratumorally. **a** Schematic showing experiment timeline. **b** Analysis of myeloid immune populations as percentage of total cells by flow cytometry. **c** Analysis of effector CD4 and CD8 T cells as determined by gating for CD44$^+$IFNγ^+. **d** Analysis of STAT3 phosphorylation levels on myeloid immune populations as measured by mean-fluorescence intensity (MFI). **e** Sub-analysis of MDSCs expressing pSTAT3 and Ki67 by flow cytometry. Students' t test was performed to assess significance between control and RT groups. Asterisks denote significance ($p < 0.05$). Bars represent standard error of the mean of 3–4 independent experiments

cells that were Ly6C^{high} and Ly6G$^+$ increased by 2.16-fold (Fig. 2b). No significant change was observed in the proportion of macrophages (CD11b$^+$F4/80$^+$) (Fig. 2b). The proportion of Tregs, CD8, and CD4 T cells remained unchanged following treatment (Supplementary Fig. 1b), but the proportion of effector T cells was significantly increased after RT, consistent with previous reports [20, 21] (Fig. 2c).

To identify possible mechanisms mediating the increased presence of immunosuppressive cells after RT, we analyzed STAT3 phosphorylation (pSTAT3) on each cell population. STAT3 is considered to be a critical factor in the regulation of myeloid cell expansion and activity [9]. At baseline, we observed the highest expression of pSTAT3 on neutrophils and G-MDSCs (MFI 17.67 and 13.47, respectively) (Fig. 2d). Tumor cells and non-immune cells (CD45$^-$) did not express pSTAT3 (Supplementary Fig. 1c). In response to RT, the mean-fluorescence intensity (MFI) of pSTAT3 was significantly increased on G-MDSCs, neutrophils, and Ly6G$^+$Ly6C$^+$ cells (Fig. 2d). In addition, pSTAT3 MFI was significantly increased on Tregs (Supplementary Fig. 1d). Furthermore, the proportion of proliferating MDSCs that express pSTAT3 was significantly increased with RT

(Fig. 2e). No significant change in pSTAT3 was observed in macrophages, total MDSC, or M-MDSCs post-RT (Fig. 2d). These data are concordant with our observation of increased G-MDSCs in PDAC patients.

Inhibition of STAT3 signaling enhances tumor response to RT

To test the therapeutic efficacy of STAT3 ASO in combination with RT, we administered STAT3 ASO in FC1242 and PK5L1940 tumor-bearing mice when average tumor volume reached 100mm^3 (days 5–6 post tumor inoculation). RT at a dose of 8 Gy was administered 72 h later and STAT3 ASO dosing was maintained for 2 weeks (Fig. 3a). We observed a significant effect only when STAT3 ASO was combined with RT when compared to control or either treatment alone. In FC1242 tumor-bearing mice, average tumor volume in the RT + STAT3 ASO group on day 29 when all mice were alive was 293.2 mm^3 as compared to 827.1 mm^3 in the RT alone group (Fig. 3b; Supplementary Fig. 2a). In PK5L1940 tumor-bearing mice, average tumor volume in the RT + STAT3 ASO group on day 24 when all

Fig. 3 STAT3 inhibition in combination with RT significantly delays tumor growth. **a** Schematic showing experiment timeline. **b**, **c** Analysis of tumor growth in FC1242 and PK5L1940 murine PDAC when treated with RT alone or in combination with STAT3 ASO. Non-parametric unpaired *t* test was used to assess significance. Asterisks denote significance between groups (*$p < 0.05$, **$p < 0.01$, ***$p < 0.001$). Bars represent SEM of 7–8 mice per group. **d** Analysis of survival in FC1242 and PK5L1940 PDAC murine tumors when treated with RT alone or in combination with STAT3 ASO. **e** Analysis of tumor growth in nude mice bearing FC1242 tumors treated with RT alone or in combination with STAT3 ASO. **f** Analysis of tumor growth in nude mice treated with RT and RT + STAT3 ASO
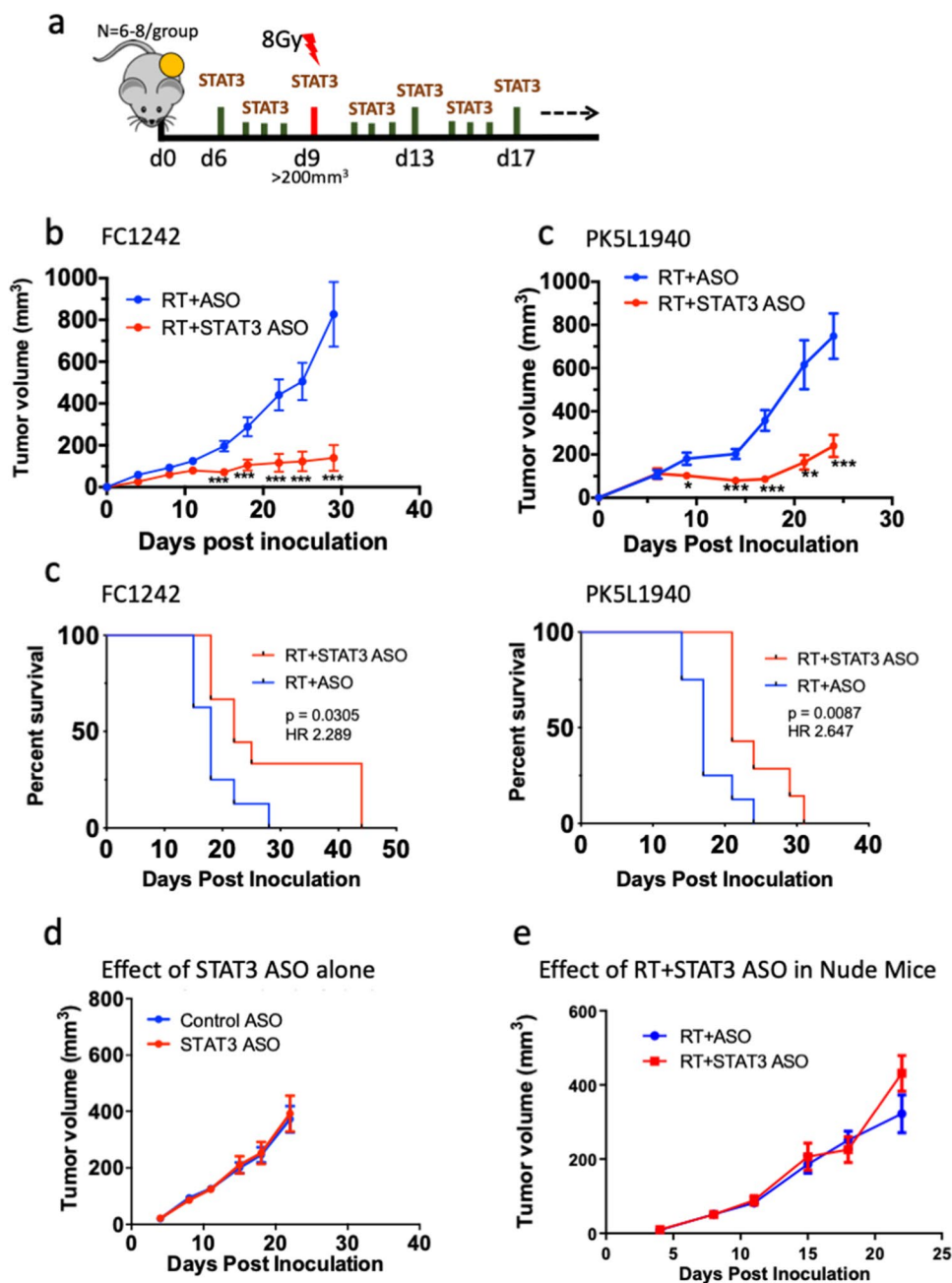
mice were alive was 240.2 mm³ relative to 748.0 mm³ in the RT alone group (Fig. 3c; Supplementary Fig. 2b). Treatment with STAT3 ASO in combination with RT also improved survival over RT alone in both cell lines (Fig. 3d). However, STAT3 ASO treatment alone did not significantly affect tumor growth in PK5L1940 tumor-bearing mice when compared to the control ASO alone group (Fig. 3e; Supplementary Fig. 2c). To determine whether the potent response we observed to STAT3 ASO and RT treatment was T cell mediated, we implanted FC1242 tumors in nude mice of the same strain (C57BL/6). The effect of combination RT and STAT3 ASO was completely reversed in nude mice, indicating T

cells are indispensable for the therapeutic efficacy of STAT3 ASO and RT (Supplementary Fig. 2d). Taken together, these data provide evidence for the therapeutic efficacy of STAT3 inhibition when combined with RT.

STAT3 blockade reverses RT-induced immunosuppression and promotes anti-tumor immunity

In order to determine the effect of combination RT and STAT3 ASO on intratumoral immunosuppressive populations, we performed flow cytometry on tumors harvested

from mice that were allowed to develop FC1242 tumors for 2-weeks and then treated with STAT3 ASO alone or in combination with RT (Fig. 4a). ASO control and RT alone groups were used as controls. Tumors were harvested 72 h following the initiation of treatment to determine the early effects of STAT3 ASO on the tumor immune microenvironment. We observed a significant decrease in pSTAT3 expression on the total MDSCs and neutrophils in the STAT3 ASO and RT + STAT3 ASO (Fig. 4b). pSTAT3 MFI on neutrophils decreased by 1.7 and 1.6 fold in the RT + STAT3 ASO group relative to ASO and RT, respectively. In the MDSC population, pSTAT3 MFI decreased by 1.7 and 1.8 fold in the RT + STAT3 ASO group relative to ASO control and RT control groups, respectively. pSTAT3 MFI on macrophages did not change significantly between groups. Consistent with the decrease in pSTAT3 expression, we observed a significant decrease in total MDSCs and neutrophils, while macrophages did not change significantly (Fig. 4c). Subgating of MDSCs into granulocytic (CD11b$^+$Ly6C^{lo}Ly6G$^+$) and monocytic (CD11b$^+$Ly6C^{hi}Ly6G$^-$) showed that treatment with STAT3 ASO reversed RT-induced expansion of intratumoral G-MDSCs (Fig. 4d). The proportion of G-MDSCs decreased by 3.1 and 8.7 fold in the

RT + STAT3 ASO group relative to the control ASO and control RT groups respectively. Similarly, the proportion of Ly6G$^+$Ly6C$^+$ cells decreased by 1.2 and 2.5 fold in the RT + STAT3 ASO group relative to the control ASO and control RT groups, respectively. Although total macrophages did not change significantly, the proportion of M1 macrophages (CD11b$^+$F4/80$^+$iNOS$^+$) was significantly increased in the RT and RT + STAT3 ASO groups, while the proportion of M2 macrophages (CD11b$^+$F4/80$^+$CD163$^+$) significantly decreased in the RT + STAT3 ASO group and significantly increased in the RT alone group (Fig. 4e) This resulted in a significantly increased M1:M2 ratio in the combination group only (Supplementary Fig. 3a). These data show a potent effect for STAT3 ASO in mediating a selective decrease of pSTAT3 expression on G-MDSCs and neutrophils as well as a decrease in their intratumoral presence.

We further assessed the effect of combination RT and STAT3 ASO on regulatory T cells (FoxP3$^+$) and activated effector T cells (CD44$^+$IFNγ$^+$). Tumors treated with RT and STAT3 ASO had significantly decreased Tregs compared to control ASO and control RT groups (2.2 and 1.9 fold decrease respectively) (Fig. 4f). Similarly, Treg pSTAT3 expression was significantly decreased following
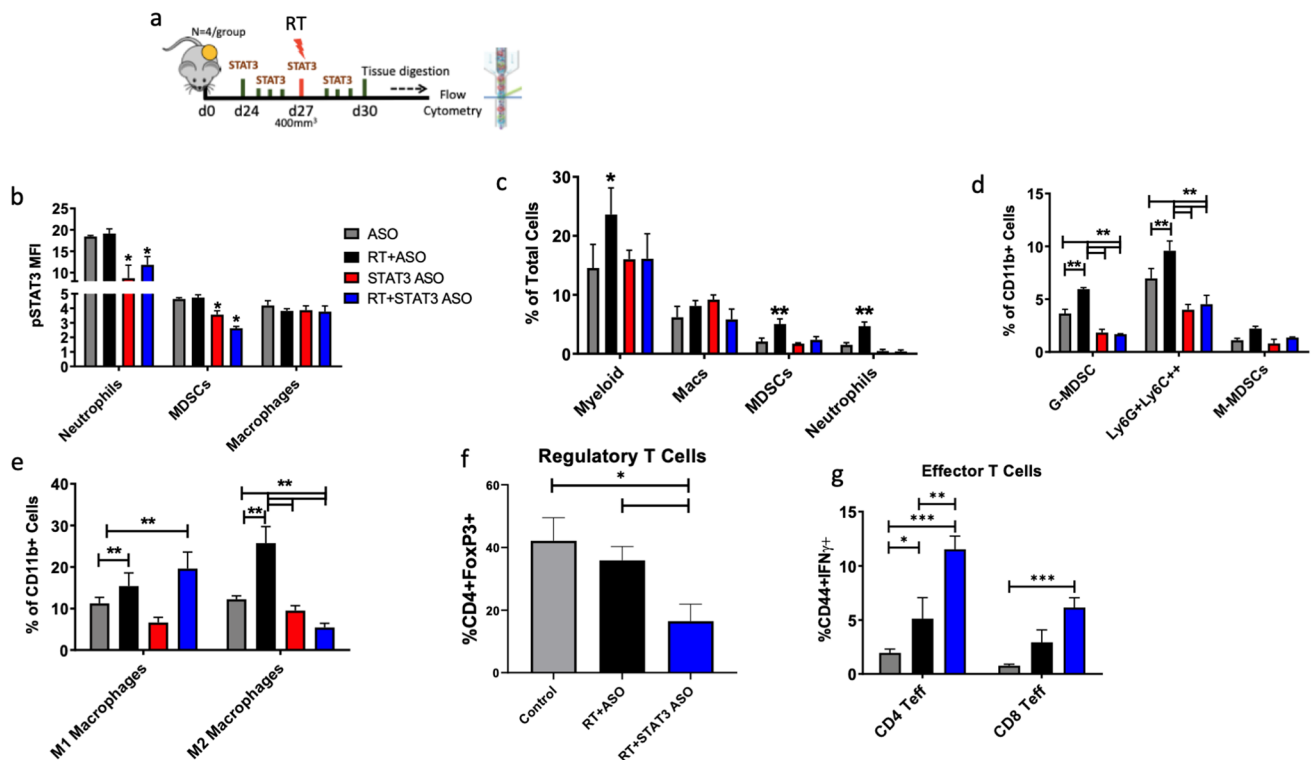
Fig. 4 STAT3 ASO mitigates RT-induced MDSC infiltration in PDAC murine tumors. **a** Schematic showing experiment timeline. **b** Analysis of intratumoral STAT3 phosphorylation on myeloid immune populations as measured by mean-fluorescence intensity (MFI). **c** Analysis of parent myeloid immune populations as percentage of total cells by flow cytometry in murine FC1242 tumors. **d**, **e** Analysis of intratumoral MDSC and macrophage sub-populations. **f** Analysis of intratumoral regulatory T cells. **g** Analysis of intratumoral effector T cells

combination treatment (Supplementary Fig. 3b). In contrast, we observed a significant increase in effector CD4^{+} and CD8^{+} T cells in the RT + STAT3 ASO group compared to control or RT alone (Fig. 4g). Taken together, our data demonstrate that STAT3 ASO in combination with RT decreases intratumoral immune suppression and enhances effector T cell function.

Inhibition of STAT3 signaling reduces RT-induced intratumoral fibrosis

STAT3 has been shown to be a critical regulator of fibrosis in models of epithelial injury [22]. We therefore tested the effect of STAT3 inhibition with and without RT on fibrosis (Fig. 5a). Treatment with STAT3 ASO in combination with RT resulted in a significant decrease in fibrosis and collagen deposition intratumorally as assessed by Masson's Trichrome and PicroSirius Red staining, respectively (Fig. 5b, c). We further assessed plasma levels of the pro-fibrotic marker transforming growth factor-β1 (TGF-β1) from the blood of FC1242 tumor-bearing mice. TGF-β1 is the predominant factor responsible for activation of canonical and non-canonical pathways that drive myofibroblast activation, ECM production, and inhibition of ECM degradation [23]. Consistent with the decrease in mature collagen, we observed a twofold decrease in TGF-β1 as determined by ELISA on plasma samples from mice treated with RT and STAT3 ASO compared to RT alone (Fig. 5d). We further assessed ECM differences between RT and RT + STAT3 ASO treatment using mass-spectrometry. FC1242 tumors were assessed 1 week after the initiation of STAT3 ASO dosing and 3 days after RT (Fig. 5e). Two proteins were significantly increased by RT + STAT3 ASO relative to RT (Arf1 and Igf2r) and 7 proteins were significantly decreased with RT + STAT3 ASO relative to RT (Sdc1, Kng2, Pum1, Acta2, Zc3h14, Hnmpd and Sf3b5). Among the proteins that decreased with the addition of STAT3 ASO, Syndecan-1 (Sdc1) has been shown to play an important role in ECM remodeling and collagen deposition and its inhibition suppresses inflammatory responses [24]. In addition to Sdc1, Smooth muscle alpha actin (Acta2) plays a pro-fibrotic role in the ECM and its expression was significantly decreased
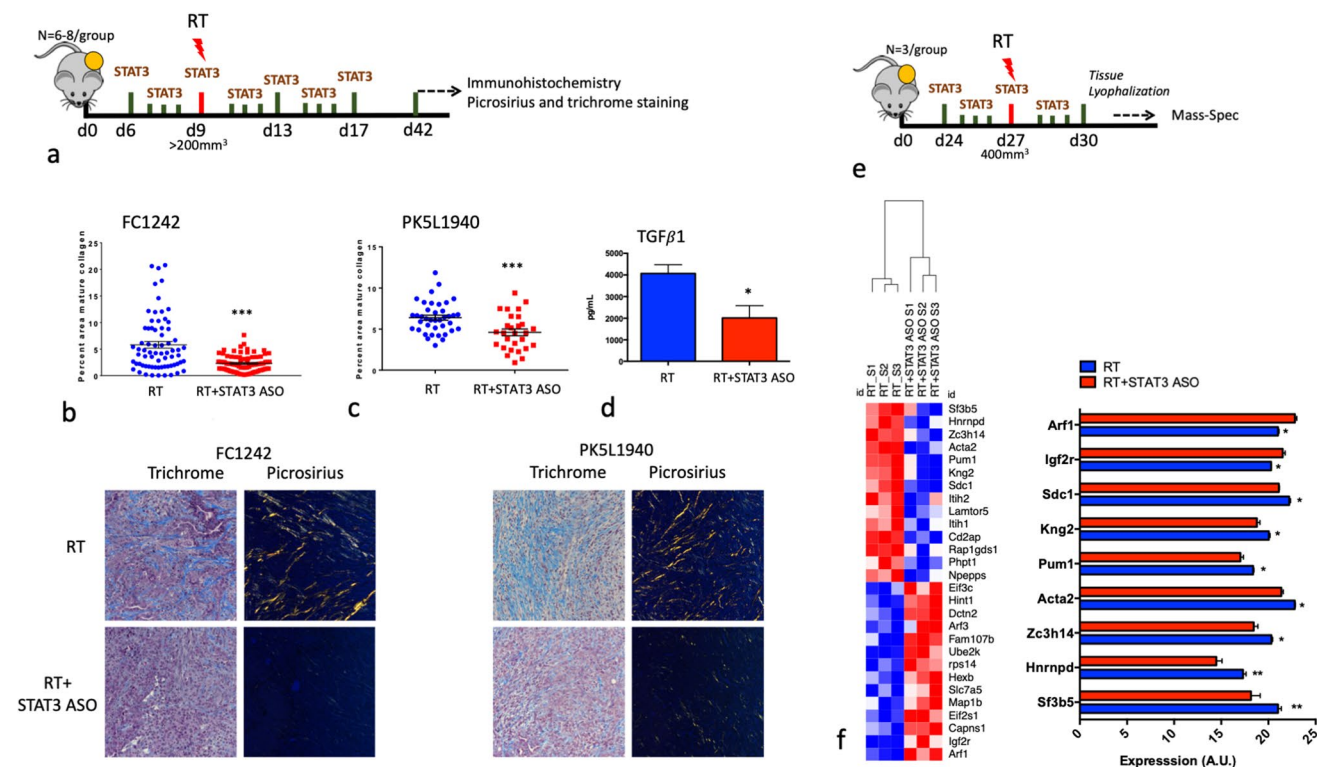
Fig. 5 Treatment with STAT3 ASO in combination with RT reduces collagen deposition. **a** Schematic of experiment timeline. **b, c** Analysis of mature collagen by PicroSirius and trichrome staining in FC1242 and PK5L1940 tumors. Quantification was performed based on picrosirius staining. Masson's stains collagen in blue and keratin and muscle fibers in red. PicroSirius images were acquired through polarized light to mark collagen. Representative images for each staining are shown below the graphs. $n = 3–5$ tumors per group, 5–8 images per tumor. **d** Analysis of TGF-β1 serum levels in FC1242 tumor-bearing mice treated with RT alone and in combination with STAT3 ASO. **e** Schematic of experimental (Refer timeline). **f** Mass spectrometry analysis of gene expression changes on tumors treated with RT alone and in combination with STAT3 ASO

with the combination of RT and STAT3 ASO [25]. Collectively, these data show that STAT3 inhibition can significantly reduce PDAC fibrosis, a key mediator of treatment resistance in PDAC patients.

Discussion

Myeloid cells play a pivotal role in tumor progression, metastasis, and resistance to chemo- and radiotherapy [26, 27]. MDSCs, a subclass of the myeloid population, are distinct from terminally differentiated myeloid cells including macrophages and neutrophils. Within the MDSC subpopulation are immature mononuclear cells, which are morphologically and functionally similar to monocytes and therefore known as M-MDSCs, and immature polymorphonuclear cells, which are morphologically and functionally similar to neutrophils and therefore known as granulocytic MDSCs [28]. Although their precise role remains controversial, MDSCs have been shown to play a key role in tumor progression by regulating not only T [29] and NK [30] cell anti-tumor activity, but also in promoting tumor neovascularization [31], neoplastic cell invasion in the surrounding tissues [32], and the seeding of neoplastic cells in distant sites [33]. Several mechanisms mediate MDSC's suppression of immune cell function including: expression of arginase [34], TGF-β [30], IL-10 [26], and COX2 [35], sequestration of cysteine [36], decreased expression of L-selectin by T cells [37], and induction of Tregs [38]. Through such mechanisms, MDSCs can protect tumor cells from immune-mediated killing.

Most effects of RT on the TME involve the recruitment and repolarization of tumor-promoting immunosuppressive cells, making depletion of TAMs, MDSCs, and other myeloid cells an attractive therapeutic approach to combine with RT [39]. However, these treatments may have off-target effects and inadvertently deplete dendritic cells (DCs) or M1-polarized TAMs that are essential for effective anti-tumor immunity. New therapeutic agents are warranted that are aimed at leveraging the synergy with radiation while countering its negative effect. In our study, RT further induced the already prevalent G-MDSC population in murine PDAC tumors and patient samples. With the advent of various immunotherapy regimens, employing RT in combination with immune therapies that limit MDSC activation and promote effector T cell responses, will be important. In that respect combining STAT3 ASO and anti-PD-1 is an appealing next step.

Considerable evidence indicates that the STAT3 pathway in myeloid cells may be crucial for MDSC differentiation, survival, and function [40]. Our data show that MDSCs, and in particular G-MDSCs, express the highest levels of STAT3 phosphorylation compared to all other myeloid

subtypes and these levels are further increased by RT. Treatment with STAT3-ASO reversed RT-induced STAT3 phosphorylation and decreased MDSC proliferation. However, despite STAT3 ASO's ability to significantly reduce intratumoral MDSC and neutrophil accumulation, we show that it is insufficient in inducing effector T cell infiltration and activation. When combined with RT, STAT3 ASO achieves two important functions: reversing RT-induced immune suppression and enabling accumulation of effector T cells which are indispensable for anti-tumor immunity. Additionally, RT has been shown in multiple studies to either increase Treg intratumoral recruitment or unable to override it [41]. We show that combination RT and STAT3 ASO treatment yields a significant decrease in Tregs. STAT3 has also been previously demonstrated to act as a co-transcription factor with FOXP3, therefore decreasing their conversion to Tregs [42]. Our results are supportive of this hypothesis as there is significant percent increase in CD4 Teff accompanying the reduction of Tregs when anti-STAT3-ASO is combined with RT.

Several cancer-derived cytokines and growth factors including IL-6, IL-10, TGF-β1, CCL2, have also been reported to support the expansion of MDSCs and Tregs in the TME through STAT3 signaling [28]. CCL2 mediated signaling, for example, has been shown to recruit MDSCs to the TME following RT, and abrogation by genetic or pharmacologic inhibition of CCR2 restores response to RT [43]. Our patient data show RT results in persistent elevation of CCL2, VEGF, TGF-β1, among other cytokines. These effects correlated with progressive accumulation of G-MDSCs. These data are consistent with previously published results in patients undergoing RT in different tumor types [44] and are likely mediated via production of ROS by RT [28]. In addition, to the role that TGF-β1 plays in the differentiation of MDSCs, it has an established role in regulating pancreatic epithelial cell cycle through cyclin-dependent kinase inhibitors such as p21 [45]. Although TGF-β1 is generally growth inhibitory to epithelial cells [46, 47], it can promote proliferation of pancreas stellate cells [48]. In addition, TGF-β1 has been implicated in promoting both the migration of and matrix deposition by pancreas stellate cells [49]. Due to the pleiotropic effects of TGF-β1, its targeting in cancer has been challenging. Pancreas epithelium-specific genetic deletion of the TGF-β1 receptor (*Tgfbr2*) has been shown to promote tumor progression in Kras-driven PDAC animal models [50, 51]. In our studies, circulating levels of TGF-β1 were significantly reduced in response to STAT3-ASO in animals with PDAC tumors, but it is conceivable that such an effect is transient and the beneficial effects of TGF-β1 on normal pancreas epithelium are not lost.

Although previous clinical trials targeting STAT3 with small molecular inhibitors had reported limited efficacy and broad adverse effects [52], recently STAT3 anti-sense

oligonucleotide, AZD9150, demonstrated a good safety and tolerability profile and showed clinical activity as a single-agent in a phase I dose-escalation study in lung cancer [53].

The immunosuppressive TME within PDAC composed primarily of MDSCs, Tregs, TAMs, and activated fibroblasts plays an important role in the regulation of PDAC tumor growth and the dampened response to targeted therapy, including radiation. STAT3 represents a promising target in that it regulates the activation and proliferation of these immunosuppressive cell populations. Although, our experiments demonstrated an important role for STAT3 ASO in limiting MDSCs, it is conceivable that off-target effects on populations such as endothelial cells, fibroblasts and pericytes are present. Future studies exploring how STAT3 ASO affects tumor vasculature and angiogenesis will be important.

An important aspect to consider in designing therapeutic strategies is the plasticity of the tumor microenvironment and its ability to adapt to treatment-induced changes. Since MDSCs are heterogeneous but overlap in functional traits, it may be necessary to inhibit multiple immunosuppressive subsets while maintaining M1 polarization and effector T cell function to observe a therapeutic effect. While these therapies are still being assessed in clinical trials, combining radiation with anti-STAT3 inhibitors might fulfill that requirement and hold clinical promise in patients with LAPC.

Compliance with ethical standards

Ethical approval All protocols for animal tumor models were approved by the IACUC of the University of Colorado Denver. Mice exhibiting signs of morbidity according to the guidelines set by the Institutional Animal Care and Use Committee (IACUC) were sacrificed immediately.

Informed consent All human studies were performed after approval by the University of Colorado institutional review board (COMIRB16-1139) and written informed consent was obtained from all patients as dictated by the study protocol.

References

1. Garrido-Laguna I, Hidalgo M (2015) Pancreatic cancer: from state-of-the-art treatments to promising novel therapies. Nat Rev Clin Oncol 12(6):319–334
2. Siegel RL, Miller KD, Jemal A (2019) Cancer statistics, 2019. CA A Cancer J Clin 69(1):7–34
3. Bailey P et al (2016) Genomic analyses identify molecular subtypes of pancreatic cancer. Nature 531(7592):47–52
4. Li X et al (2015) Emerging immune checkpoints for cancer therapy. Acta Oncol 54(10):1706–1713
5. Huguet F et al (2007) Impact of chemoradiotherapy after disease control with chemotherapy in locally advanced pancreatic adenocarcinoma in GERCOR phase II and III studies. J Clin Oncol 25(3):326–331
6. Balogh A et al (2013) The effect of ionizing radiation on the homeostasis and functional integrity of murine splenic regulatory T cells. Inflamm Res 62(2):201–212
7. Cao M et al (2009) Gamma irradiation alters the phenotype and function of CD4+CD25+ regulatory T cells. Cell Biol Int 33(5):565–571
8. Seifert L et al (2016) Radiation therapy induces macrophages to suppress T-cell responses against pancreatic tumors in mice. Gastroenterology 150(7):1659–1672 **(e5)**
9. Gabrilovich DI, Nagaraj S (2009) Myeloid-derived suppressor cells as regulators of the immune system. Nat Rev Immunol 9(3):162–174
10. Barcellos-Hoff MH (2010) Stromal mediation of radiation carcinogenesis. J Mammary Gland Biol Neoplasia 15(4):381–387
11. Barker HE et al (2015) The tumour microenvironment after radiotherapy: mechanisms of resistance and recurrence. Nat Rev Cancer 15(7):409–425
12. Ohuchida K et al (2004) Radiation to stromal fibroblasts increases invasiveness of pancreatic cancer cells through tumor-stromal interactions. Cancer Res 64(9):3215–3222
13. Neesse A et al (2011) Stromal biology and therapy in pancreatic cancer. Gut 60(6):861–868
14. Mariathasan S et al (2018) TGFbeta attenuates tumour response to PD-L1 blockade by contributing to exclusion of T cells. Nature 554(7693):544–548
15. Petit V et al (2013) Optimization of tumor xenograft dissociation for the profiling of cell surface markers and nutrient transporters. Lab Invest 93(5):611–621
16. Hadi AM et al (2011) Rapid quantification of myocardial fibrosis: a new macro-based automated analysis. Cell Oncol (Dordr) 34(4):343–354
17. Chong J et al (2018) MetaboAnalyst 4.0: towards more transparent and integrative metabolomics analysis. Nucleic Acids Res 46(W1):W486–W494
18. Hillmer EJ et al (2016) STAT3 signaling in immunity. Cytokine Growth Factor Rev 31:1–15
19. Cursiefen C et al (2004) VEGF—a stimulates lymphangiogenesis and hemangiogenesis in inflammatory neovascularization via macrophage recruitment. J Clin Investig 113(7):1040–1050
20. Garnett CT et al (2004) Sublethal irradiation of human tumor cells modulates phenotype resulting in enhanced killing by cytotoxic T lymphocytes. Cancer Res 64(21):7985–7994
21. Lennon S et al (2019) Pancreatic tumor microenvironment modulation by EphB4-ephrinB2 inhibition and radiation combination. Clin Cancer Res 25(11):3352–3365
22. Chakraborty D et al (2017) Activation of STAT3 integrates common profibrotic pathways to promote fibroblast activation and tissue fibrosis. Nat Commun 8(1):1130
23. Meng XM, Nikolic-Paterson DJ, Lan HY (2016) TGF-beta: the master regulator of fibrosis. Nat Rev Nephrol 12(6):325–338

24. Lei J et al (2013) Sdc1 overexpression inhibits the p38 MAPK pathway and lessens fibrotic ventricular remodeling in MI rats. Inflammation 36(3):603–615

25. Rockey DC, Weymouth N, Shi Z (2013) Smooth muscle alpha actin (Acta 2) and myofibroblast function during hepatic wound healing. PLoS One 8(10):e77166

26. Hu CE et al (2011) Up-regulated myeloid-derived suppressor cell contributes to hepatocellular carcinoma development by impairing dendritic cell function. Scand J Gastroenterol 46(2):156–164

27. Lesokhin AM et al (2012) Monocytic CCR2(+) myeloid-derived suppressor cells promote immune escape by limiting activated CD8 T-cell infiltration into the tumor microenvironment. Cancer Res 72(4):876–886

28. Marvel D, Gabrilovich DI (2015) Myeloid-derived suppressor cells in the tumor microenvironment: expect the unexpected. J Clin Investig 125(9):3356–3364

29. Marigo I et al (2008) Tumor-induced tolerance and immune suppression by myeloid derived suppressor cells. Immunol Rev 222:162–179

30. Li H et al (2009) Cancer-expanded myeloid-derived suppressor cells induce anergy of NK cells through membrane-bound TGF-beta 1. J Immunol 182(1):240–249

31. Murdoch C et al (2008) The role of myeloid cells in the promotion of tumour angiogenesis. Nat Rev Cancer 8(8):618–631

32. Dolcetti L, Peranzoni E, Ugel S, Marigo I, Fernandez Gomez A, Mesa C, Geilich M, Winkels G, Traggiai E, Casati A et al (2010) Hierarchy of immunosuppressive strength among myeloid-derived suppressor cell subsets is determined by GM-CSF. Eur J Immunol 40(1):22–35

33. Condamine T et al (2015) Regulation of tumor metastasis by myeloid-derived suppressor cells. Annu Rev Med 66:97–110

34. Movahedi K et al (2008) Identification of discrete tumor-induced myeloid-derived suppressor cell subpopulations with distinct T cell-suppressive activity. Blood 111(8):4233–4244

35. Mao Y et al (2013) Melanoma-educated CD14+ cells acquire a myeloid-derived suppressor cell phenotype through COX-2-dependent mechanisms. Cancer Res 73(13):3877–3887

36. Srivastava MK et al (2010) Myeloid-derived suppressor cells inhibit T-cell activation by depleting cystine and cysteine. Cancer Res 70(1):68–77

37. Hanson EM et al (2009) Myeloid-derived suppressor cells downregulate L-selectin expression on CD4+ and CD8+ T cells. J Immunol 183(2):937–944

38. Lindau D et al (2013) The immunosuppressive tumour network: myeloid-derived suppressor cells, regulatory T cells and natural killer T cells. Immunology 138(2):105–115

39. Gough MJ, Young K, Crittenden M (2013) The impact of the myeloid response to radiation therapy. Clin Dev Immunol 2013:281958

40. Yu H, Pardoll D, Jove R (2009) STATs in cancer inflammation and immunity: a leading role for STAT3. Nat Rev Cancer 9(11):798–809

41. Oweida AHM, Phan A, Binder D, Bhatia S, Lennon S, Bukkapatnam S, Vancourt B, Uyanga N, Darragh L, Kim HM, Raben D, Tan AC, Heasley L, Clambey E, Nemenoff R, Karam SD (2018) Resistance to radiotherapy and PD-L1 blockade is mediated by TIM-3 upregulation and regulatory T-cell infiltration. Clin Cancer Res 24:5368–5380

42. Hossain DM et al (2013) FoxP3 acts as a cotranscription factor with STAT3 in tumor-induced regulatory T cells. Immunity 39(6):1057–1069

43. Liang H et al (2017) Host STING-dependent MDSC mobilization drives extrinsic radiation resistance. Nat Commun 8(1):1736

44. Yako YY et al (2016) Cytokines as biomarkers of pancreatic ductal adenocarcinoma: a systematic review. PLoS One 11(5):e0154016

45. Bauer J et al (2012) Effects of activin and TGFbeta on p21 in colon cancer. PLoS One 7(6):e39381

46. Miyazono K (2000) Positive and negative regulation of TGF-beta signaling. J Cell Sci 113(Pt 7):1101–1109

47. Miyazono K, ten Dijke P, Heldin CH (2000) TGF-beta signaling by Smad proteins. Adv Immunol 75:115–157

48. Apte MV et al (1999) Pancreatic stellate cells are activated by proinflammatory cytokines: implications for pancreatic fibrogenesis. Gut 44(4):534–541

49. Shek FW et al (2002) Expression of transforming growth factor-beta 1 by pancreatic stellate cells and its implications for matrix secretion and turnover in chronic pancreatitis. Am J Pathol 160(5):1787–1798

50. Ijichi H et al (2006) Aggressive pancreatic ductal adenocarcinoma in mice caused by pancreas-specific blockade of transforming growth factor-beta signaling in cooperation with active Kras expression. Genes Dev 20(22):3147–3160

51. Kojima K et al (2007) Inactivation of Smad4 accelerates Kras(G12D)-mediated pancreatic neoplasia. Cancer Res 67(17):8121–8130

52. Bendell JC et al (2014) Phase 1, open-label, dose-escalation, and pharmacokinetic study of STAT3 inhibitor OPB-31121 in subjects with advanced solid tumors. Cancer Chemother Pharmacol 74(1):125–130

53. Hong D et al (2015) AZD9150, a next-generation antisense oligonucleotide inhibitor of STAT3 with early evidence of clinical activity in lymphoma and lung cancer. Sci Transl Med 7(314):314ra185

Affiliations

Ayman J. Oweida[1] · Adam C. Mueller[11] · Miles Piper[10] · Dallin Milner[10] · Benjamin Van Court[10] · Shilpa Bhatia[10] · Andy Phan[10] · Thomas Bickett[10] · Kimberly Jordan[9] · Theresa Proia[2] · Richard Schulick[3] · Wells A. Messersmith[4] · Marco Del Chiaro[3] · Eric Clambey[5] · Michael J. Gough[6] · Jason Williams[7] · Kirk Hansen[7] · Karyn Goodman[8] · Sana D. Karam[1,10] [ORCID]

1. Department of Nuclear Medicine and Radiobiology, University of Sherbrooke, Sherbrooke, Canada

2. Bioscience, Oncology, IMED Biotech Unit, AstraZeneca, Boston, MA, USA

3. Department of Surgery, University of Colorado Anschutz Medical Campus, Aurora, CO, USA

4. Division of Medical Oncology, Department of Medicine, University of Colorado Anschutz Medical Campus, Aurora, CO, USA

5 Department of Anesthesiology, University of Colorado Anschutz Medical Campus, Aurora, CO, USA

6 Earle A. Chiles Research Institute, Providence Medical Center, Portland, OR, USA

7 Department of Biochemistry, University of Colorado Anschutz Medical Campus, Aurora, CO, USA

8 Department of Radiation Oncology, Icahn School of Medicine at Mount Sinai, New York, NY, USA

9 Department of Immunology and Microbiology, University of Colorado Anschutz Medical Campus, Aurora, CO, USA

10 Department of Radiation Oncology, University of Colorado Anschutz Medical Campus, 1665 Aurora Court Suite 1032, Aurora, CO 80045, USA

11 Thomas Jefferson University, Bodine Center for Cancer Treatment, 1665 Aurora Court Suite 1032, Philadelphia, PA, USA